Exploring Insertion Reaction Dynamics: A Case Study of $S(^1D) + D_2 \rightarrow SD + D$

Shih-Huang Lee and Kopin Liu*

Institute of Atomic and Molecular Sciences (IAMS), Academia Sinica, Taipei, Taiwan 10764

Received: July 30, 1998; In Final Form: September 9, 1998

The Doppler-selected time-of-flight method was applied to map out the differential cross section of the title reaction at a collision energy of 5.3 kcal/mol. The angular distribution is highly forward/backward peaking with very slight asymmetry in favor of the forward direction. Vibrational structures of the SD product are resolved in the angle-specific translational energy distribution. A strong coupling between the product angular and speed distributions is found. Phase-space theory gives a fair description about the product translational energy distribution, though significant discrepancies are noted for angular and angle-specific speed distributions. Possible reasons are given, which consequently suggest ways for further theoretical investigation.

I. Introduction

Insertion is an important reaction pathway, which is characterized by a *simultaneous* one-bond rupture and two-bonds formation process in forming the intermediate complex. Yet, compared to the remarkable achievement that has been made over the past decades toward our basic understanding of a direct abstraction or an exchange reaction,[1−4] much less is known about its detailed dynamics. Until very recently, the reaction of $O(^1D) + H_2$ has often been regarded as a benchmark system for studying insertion dynamics. Within the past few years, however, substantial evidence from both experiments[5] and high-level ab initio potential energy surface (PES)[6] and quasiclassical trajectory (QCT) calculations[7,8] has emerged, which indicates that the reaction of $O(^1D) + H_2$ is complicated by an additional abstraction pathway proceeding on excited surfaces. The presence of a small, collinear barrier (∼2 kcal/mol) for the abstraction pathway[5,6] not only makes the direct comparison between theory and experiment for this particular reaction more challenging but also restricts one from further detailed studies of insertion dynamics in general, e.g., how the dynamics changes as the initial collision energy increases.

The reaction of $O(^1D) + H_2$ is very exoergic, ∼43 kcal/mol. As one goes down the periodic table for X, because of the weakening of the X−H bond the exothermicity of the $X + H_2$ reaction decreases. As such, the exoergicity of the title reaction reduces to 6.2 kcal/mol. (Part of the reduction in exoergicity also comes from the energy difference in electronic excitations of the $S(^1D)$ and $O(^1D)$ state.) Since the activation energy usually increases with decreasing exoergicity (the so-called Evans−Polanyi relationship,[9] sometimes also referred to as the Hammond postulate[10]), one might then anticipate the collinear abstraction barrier for the title reaction to be much higher than that for $O(^1D) + H_2$. If so, then the reaction of $S(^1D) + H_2$ could offer a better opportunity for in-depth exploration of insertion dynamics over a wider energy range. This expectation is nicely borne out from a recent excitation function measurement,[11] which strongly suggests that the reactive cross section for the title reaction can be entirely attributed to insertion for collision energies up to ca. 6 kcal/mol, the highest energy achieved in the experiment.

Reported here is our attempt to better understand the detailed insertion dynamics for this reaction. The Doppler-selected time-of-flight (TOF) technique[12] was employed to measure the doubly differential cross section, $I(\theta, v)$. In brief, to measure a 3D product velocity distribution, $I(v_x, v_y, v_z)$, the Doppler-shift technique is used in selecting a subgroup of products with $v_z \pm \delta v_z$. Rather than collecting all those signals from a resonance-enhanced multiphoton ionization (REMPI) detection process as a single data point in the conventional approach, those Doppler-selected ions are dispersed both spatially (in v_x) and temporally (in v_y). A slit placed in front of the detector restricts only those ions with $v_x \approx 0$ to be detected, and the v_y distribution of those v_x- and v_z-selected ions is then measured by the ion TOF method. To take advantage of the cylindrical symmetry of product 3D velocity distribution around the initial velocity axis ($\hat{v}_z$) in a crossed-beam scattering experiment, the parallel configuration (the probe laser propagates along $\hat{v}_z$ for Doppler selection) was adopted in this approach. Since both the Doppler slice and the ion TOF measurement are essentially in the center-of-mass (c.m.) frame and the v_x-component associated with the c.m. velocity can be made negligibly small compared to the Newton sphere, the measurement thus directly maps out the desired c.m. distribution ($d^3\sigma/v^2 dv d\Omega$, expressed in polar coordinate by convention) in a Cartesian velocity coordinate ($d^3\sigma/dv_x dv_y dv_z$).

II. Experimental Results and Analysis

The experiments were conducted in a pulsed, crossed-beam apparatus described previously.[13] The $S(^1D)$ beam was generated by 193 nm photolysis of CS_2 (0.5% in He) at the throat of a pulsed valve, and the 3D velocity distribution of the D-atom product was interrogated by the Doppler-selected TOF method. The experimental setup and procedures can be found elsewhere.[12,14,15] Figure 1a shows a typical Doppler profile of the D-atom from the title reaction at $E_c = 5.3$ kcal/mol. A prominent double-hump feature is seen with slight preference for forward-scattered products. (Note that the direction of the product being detected (D-atom) is referred to the c.m. direction of the reactant D_2 from which the D-atom originates, see ref 16 for details.) Similar bias toward forward scattering has also been observed for the other isotopic variant[17] and for the analogous reaction of $O(^1D) + D_2/H_2$ at low collision energies (<2 kcal/mol).[18,19]

Figure 1b shows a few examples of Doppler-selected TOF

10.1021/jp983220w CCC: $15.00
Published on Web 10/09/1998

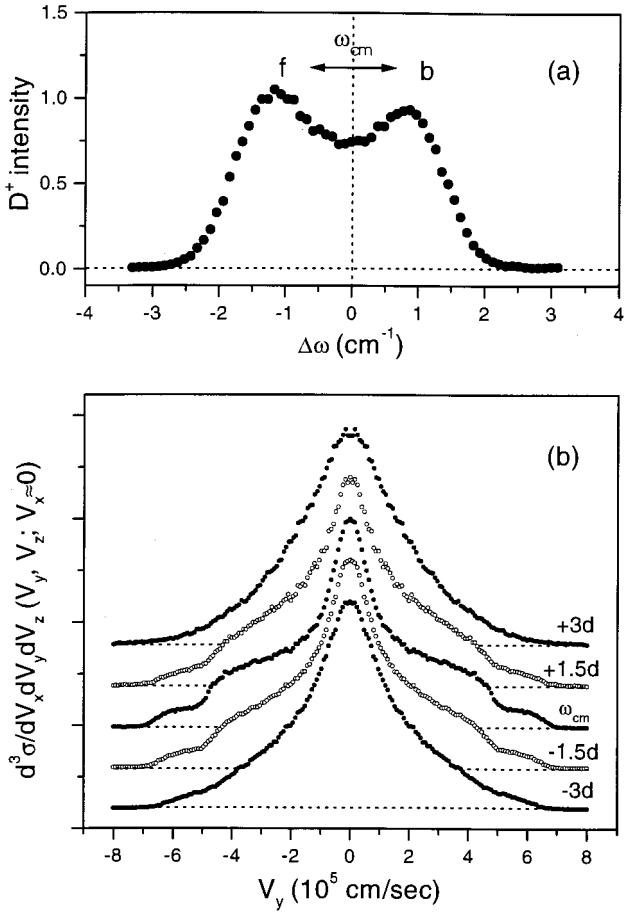

Figure 1. (a) Doppler profiles for the title reaction at $E_c = 5.3$ kcal/mol (●), obtained under the parallel configuration. The dotted line marks the partition between the forward (f) and backward (b) hemispheres for the $^2S_{1/2} \rightarrow {}^2P_{3/2}$ transition of the L-α doublet. (b) A few examples of the Doppler-selected TOF spectra of the D-atom product obtained under the ion extraction field of 1.95 V/cm. The label "ω_{cm}" corresponds to the VUV laser frequency that slices through the Newton sphere near c.m., and each "d" corresponds to 0.365 cm^{-1} in frequency or $v_z = 1.335 \times 10^5$ cm/s.

spectra. The spectra have been converted into velocity space with the apparatus function being accounted for.[12,14] Clear step-structures are vividly seen, and their appearance and position are sensitive to the initial v_z-selection. The Doppler profile of the D-atom spans over 4 cm^{-1} in width. The TOF measurements were performed for a total of about 24 equally spaced Doppler selections to cover the entire profile. By combining those data together (after the L-α doublet complication is removed[14]), the entire 3D velocity distribution can be mapped out. The resulting 3D representation of the velocity−flux contour map ($d^2\sigma/dvd(\cos\theta)$) for the D-atom product is depicted in Figure 2. A strong coupling of the product angular and speed distribution is readily observed. For example, the step structures are quite prominent for sideward-scattered products, but they merge together as the scattering angle shifts toward the forward/backward direction.

The results of a global analysis of the contour are presented in Figure 3. The product translational energy distribution, $P(E_t) = d\sigma/dE_t$, is rather broad. Also marked on the top is the onset of the vibrational state of the SD product. The vibrational structure is barely discernible at this level of detail, and a small tail, due to the finite instrument resolution, beyond the energetic limit is noted. The fraction of the average translational energy release $\langle f_t \rangle = 0.49$ is in reasonable agreement with the phase-space theoretical prediction 0.53, vide infra. Previously, using

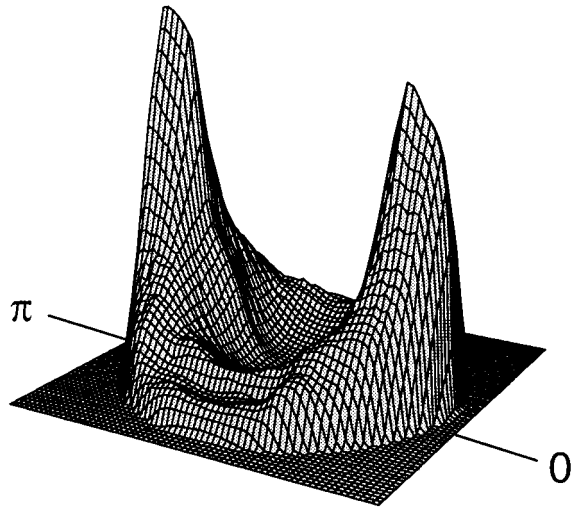

Figure 2. D-atom velocity−flux contour, $d^2\sigma/dvd(\cos\theta)$. The contours are constructed directly from a total of 24 slices of the Doppler-selected TOF measurements.

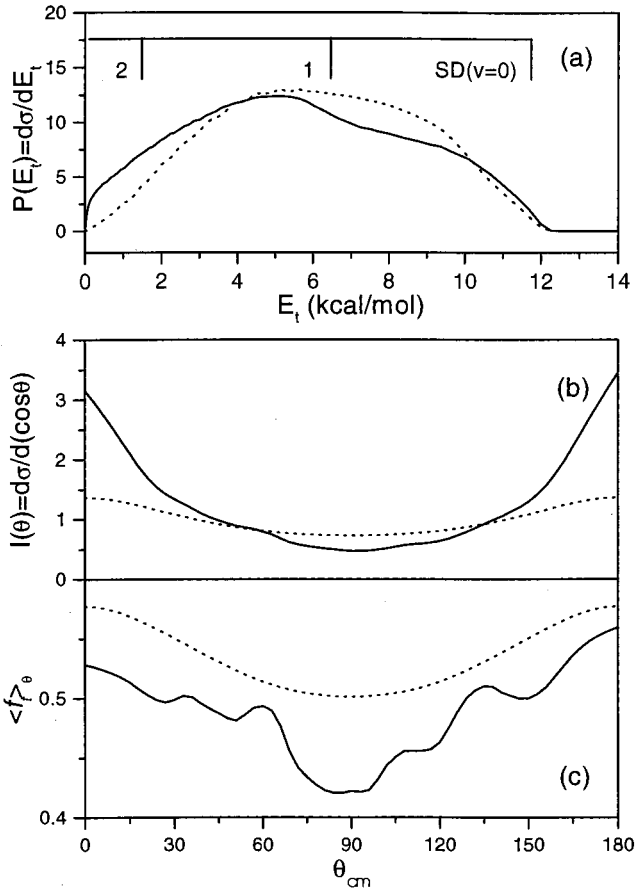

Figure 3. Comparisons of (a) the product translational energy distributions $P(E_t) = d\sigma/dE_t$, (b) the product c.m. angular distributions $d\sigma/d(\cos\theta)$, and (c) the fraction of the average translational energy release derived from the experiment (solid lines) and from the PST calculation (dotted lines). Also marked in (a) is the onset of the vibrational state of the SD product.

the second moment analysis of the observed Doppler profile in a bulk experiment, Inagaki et al. obtained $\langle f_t \rangle = 0.65 \pm 0.05$ at $\langle E_c \rangle = 4.1$ kcal/mol,[20] which is significantly larger than ours. The slight difference in E_c's cannot account for that because our result at $E_c = 2.3$ kcal/mol yields an even smaller value of 0.44.[17] One plausible explanation for the discrepancy lies on the fact that Inagaki et al. assumed an isotropic angular

distribution in the laboratory frame in their data analysis. As will be shown below, the angular distribution for this reaction is very anisotropic in the c.m. frame. Transforming it into the laboratory frame could still remain quite anisotropic, thereby invalidating their analysis.

The product c.m. angular distribution ($d\sigma/d(\cos\theta)$) is displayed in Figure 3b, which shows a pronounced f/b peaking and nearly symmetric distribution. It implies that as the insertion complex decomposes, the initial orbital angular momentum **L** (or the total angular momentum **J** as in the present study) is preferentially disposed into the final orbital angular momentum **L′**, i.e., $\mathbf{L} \approx \mathbf{J} \approx \mathbf{L}'$.[21,22] A closer examination reveals slight asymmetry. Although the peak height at 180° seems slightly higher than that at 0°, the integrated flux in the forward hemisphere (0−90°) is actually favored over that in the backward hemisphere, which is consistent with the Doppler profile (Figure 1a). Depicted in Figure 3c is the fraction of the average translational energy release as a function of $\theta_{c.m.}$, which gives a quantitative measure of the coupling of the product angular and speed distributions aforementioned. The striking oscillatory features deserve special attention (similar features are also noted at lower collisional energy[16]), and they might provide an important clue to unravel the main dynamical factors that govern this reaction.

Also shown in Figure 3 are the comparisons with the statistical prediction. As demonstrated from the excitation function measurement,[11] the insertion reaction of $S(^1D) + D_2$ proceeds with little barrier in either the entrance or the exit channel. It is thus ascribed to a loose transition state governed by the centrifugal barrier. By properly accounting for the energy and angular momentum conservations, a phase-space theory (PST) for the state-to-state angular distribution has previously been formulated by White and Light.[23] Using their formulism, the results of such a calculation are shown in Figure 3 as dotted lines. Here it suffices to note that the PST-calculated state-to-state differential cross sections were convoluted over the finite instrument resolutions and normalized to experiment to yield an identical integral cross section. As can be seen from Figure 3a, the PST gives a reasonable, though not perfect, account of the product translational energy distribution. Hence, if only the SD product internal state distributions were measured, one might come to the conclusion of a nearly statistical reaction governed by the PST. This is indeed the conclusion drawn from the comparison of $\langle f_t \rangle$ in the recent study by Inagaki et al.[20] However, in terms of other scattering observables such as the angular distribution (Figure 3b) or the angle-specific kinetic energy release (Figure 3c), significant discrepancies are found. The PST predicts a much milder f/b peaking angular distribution as well as a weaker coupling between product speed and angular distributions than experiment. In PST, such a $v-\theta$ coupling, or $I(v, \theta) \neq f(\theta)\, g(v)$, is the result of a purely *kinematic* requirement imposed by the angular momentum conservation. (The prior distribution in the information theoretic approach will predict a constant value of $\langle f_t \rangle = 0.51$ for all θ's.) The calculated $\langle f_t \rangle_\theta$ is consistently larger than the experiment by a small amount, part of which could arise from the exact parameters used in the present PST calculation.[17] More significantly, the observed $\langle f_t \rangle_\theta$ displays a greater angular variation for the sideward-scattered product than just from the kinematic constraint, indicative of the *dynamic* origin governed by the PES.

As presented previously,[12] a more informative way to reveal the detailed dynamics afforded by this direct 3D mapping approach is to examine the angle-specific product state distribution $P(E_t; \Delta\theta)$ over a limited range of $\Delta\theta$, as illustrated in Figure 4. For the purpose of this communication the full angle range is partitioned into only six segments. Quite remarkably, even under such a coarse-grained presentation vibrational structures become quite apparent, and their dependence on the c.m. scattering angle of the SD products is noticeable. From the envelope of these vibrational structures, the main feature in the rotational distribution can also be inferred. Qualitatively, the f/b components tend to be rotationally hotter than the sideward-scattered SD products. More quantitative rovibrational analysis is a task of some proportions and is currently in progress. The comparison with the PST prediction at this level of details (Figure 4) provides a deeper view of the discrepancy observed in Figure 3. The differences in the relative magnitude reflect the discrepancy in angular distribution shown in Figure 3b. In terms of the shape of the kinetic energy distribution in each angular segment, it appears that the PST gives a reasonable description in the forward/backward direction, but it fails to reproduce the observed product state distribution for the sideward-scattered product. Apparently, the small difference in the angle-integrated $P(E_t)$ distributions (Figure 3a) originates mostly from the marked discrepancy in the sideward direction.

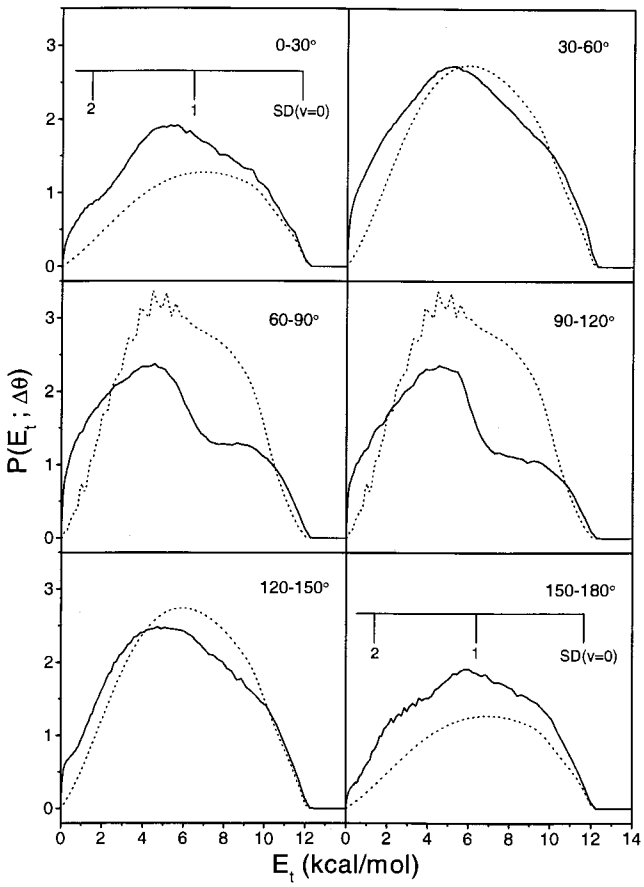

Figure 4. Angle-specific translational energy distributions over every 30° angular range, $P(E_t; \Delta\theta)$, obtained from the experiment (solid lines) and from the PST calculation (dotted lines). Experimentally, the vibrational structures are visible, and their relative magnitude and shape depend on the c.m. angle.

III. Discussion

The failure of the PST in describing all aspects of scattering observables is not too surprising. First, the PST puts no constraints on the structure of the transition state or the type of modes for dissociation of the intermediate complex. The only PES information invoked is the energetics. That is certainly

an oversimplified picture, particularly for the more detailed scattering observable. Our use of PST here is primarily a means to ensure the angular momentum conservation is being properly treated in the spirit of statistical theories, and in view of the available PES information.

Second, the PST approach assumes a long-lived complex, i.e., the lifetime of the intermediate complex is longer than the complex rotational period. As was pointed out recently,[11] the notion (in the usual sense) of a long-lived complex for the title reaction[20] is not fully consistent with the observed isotope effect. For a rotationally cold reagent, the approximation $\mathbf{L} \approx \mathbf{J}$ holds. Since **J** is a conserved quantity, the lifetime of the complex (or the unimolecular decay rate constant) should be expressed as $\tau(E, \mathbf{J})$, as emphasized by Quack and Troe quite sometime ago[24] and more recently also by Pollak and Schlier.[25,26] Hence, for a given total energy E, there will be *a distribution of complex lifetimes which depend on the initial impact parameter*, recalling that $J \approx L = \mu v b$. In other words, even for a complex-forming reaction some memory about the initial impact parameter will be retained through the angular momentum conservation. The commonly accepted concept about the lifetime of a collision complex may be considered as an ensemble-averaged (over the initial impact parameter) value. The notion of a distribution of complex lifetimes also makes a continuous link from a direct reaction to a truly long-lived (i.e., long-lived for all impact parameter collisions) complex-forming reaction. Many dynamical attributes normally associated with a direct reaction could then manifest themselves in some scattering observables for a typical complex-forming reaction. Aside from the influences of the potential well, the initial impact parameter (or the total angular momentum) plays just as a crucial role in determining the outcomes of an (insertion) complex reaction as for a direct one. The distinctions between a direct and a complex reaction could become blurred.

As hinted in this work, the angle-specific product state distribution (or the angle-angular momentum correlation) promises to be a useful diagnostic property for such an experimental probe by breaking down a swarm of reactive events into many distinct subsets of collisions, from which deeper insights into chemical reactivity could be gained. Further exploration along these lines and the full account of this work including the results at different collision energies and for other isotopomers (H_2, HD) will be reported in the future.

Acknowledgment. This work was supported by the National Science Council of Taiwan (NSC 87-2119-M-001-009-Y) and Chinese Petroleum Corp. (86-CPC-E−001-008).

References and Notes

(1) Levine, R. D.; Bernstein, R. B. *Molecular Reaction Dynamics and Chemical Reactivity*; Oxford University Press: Oxford, 1987.
(2) Polanyi, J. C. *Science* **1987**, *236*, 680.
(3) Herschbach, D. R. *Angnew. Chem., Int. Ed. Engl.* **1987**, *26*, 1221.
(4) Lee, Y. T. *Science* **1987**, *236*, 793.
(5) Hsu, Y.-T.; Wang J.-H.; Liu, K. *J. Chem. Phys.* **1997**, *107*, 2351.
(6) Ho, T.-S.; Hollebeek, T.; Rabitz, H.; Harding, L. B.; Schatz, G. C. *J. Chem. Phys.* **1996**, *105*, 10472.
(7) Schatz, G. C.; Papaioannou, A.; Peterson, L. A.; Harding, L. B.; Hollebeek, T.; Ho, T.-S.; Rabitz, H. *J. Chem. Phys.* **1997**, *107*, 2340.
(8) Schatz, G. C.; Peterson, L. A.; Kuntz, P. J. *Faraday Discuss.* **1997**, *108*, 357.
(9) Evans, M. G.; Polanyi, M. *Trans. Faraday Soc*. **1938**, *34*, 11.
(10) Hammond, G. S. *J. Am. Chem. Soc*. **1963**, *85*, 2544.
(11) Lee, S.-H.; Liu, K. *Chem. Phys. Lett.* **1998**, *290*, 323.
(12) Hsu, Y.-T.; Liu, K. *J. Chem. Phys*. **1997**, *107*, 1664.
(13) Macdonald, R. G.; Liu, K. *J. Chem. Phys.* **1989**, *91*, 821.
(14) Wang, J.-H.; Hsu, Y.-T.; Liu, K. *J. Phys. Chem.* **1997**, *101*, 6593.
(15) Wang, J.-H.; Liu, K.; Schatz, G. C.; Horst, M.*J. Chem. Phys.* **1997**, *107*, 7869.
(16) Che, D.-C.; Liu, K. *J. Chem. Phys.* **1995**, *103*, 5164.
(17) Lee, S.-H.; Liu, K., unpublished.
(18) Hermine, P.; Hsu, Y.-T.; Liu, K., in preparation.
(19) Casavecchia, P., private communication.
(20) Inagaki, Y.; Shamsuddin, S. M.; Matsumi, Y.; Kawasaki, M. *Laser Chem*. **1994**, *14*, 235.
(21) Miller, W. B.; Safron, S. A.; Herschbach, D. R. *Discuss. Faraday Soc*. **1967**, *44*, 108.
(22) Kim, S. K.; Herschbach, D. R. *Faraday Discuss. Chem. Soc*. **1987**, *84*, 159.
(23) White, R. A.; Light, J. C. *J. Chem. Phys*. **1971**, *55*, 379.
(24) Quack, M.; Troe, J. *Ber. Bunsen-Ges. Phys. Chem.* **1974**, *78*, 240.
(25) Schlier, Ch. *Mol. Phys.* **1987**, *62*, 1009.
(26) Pollak, E.; Schlier, Ch. *Acc. Chem. Res.* **1989**, *22*, 223.